THE JOURNAL OF PHYSICAL CHEMISTRY B LETTERS

2005, *109,* 18214−18217
Published on Web 09/14/2005

Interplay between Auger and Ionization Processes in Nanocrystal Quantum Dots

Robert M. Kraus, Pavlos G. Lagoudakis,* Josef Müller, Andrey L. Rogach, John M. Lupton, and Jochen Feldmann

Photonics and Optoelectronics Group, Physics Department and CeNS, Ludwig-Maximilians-Universität München, Amalienstr. 54, 80799 Munich, Germany

Dimitri V. Talapin and Horst Weller

Institute of Physical Chemistry, University of Hamburg, Grindelallee 117, 20146 Hamburg, Germany

Received: July 5, 2005; In Final Form: July 28, 2005

We study the interplay between Auger effects and ionization processes in the limit of strong electronic confinement in core/shell CdSe/ZnS semiconductor nanocrystal quantum dots. Spectrally resolved fluorescence decay measurements reveal a monotonic increase of the photoluminescence decay rate on excitation density. Our results suggest that Auger recombination accelerates ionization processes that lead to the occupation of dark, nonemissive nanocrystal states. A model is proposed in the quantized Auger regime describing these experimental observations and providing an estimate of the Auger assisted ionization rates.

The optoelectronic properties of semiconductor nanocrystal quantum dots (NQDs) bear great relevance to fundamental research in semiconductor physics.[1,2] Moreover, the tunability of their photoluminescence (PL) from ultraviolet to near-infrared wavelengths and the large absorption cross-section under nonresonant excitation render these nanostructures promising elements of future applications, e.g., in light-emitting diodes, biophysical fluorescence markers, and for biomedical sensitization purposes.[3−5] It is therefore important to understand the nature of spontaneous emission and competing nonradiative decay channels in these materials.

The most significant nonradiative processes that reduce the quantum efficiency of NQDs are thermal ionization or tunneling of a carrier to a trap state and Auger effects. In semiconductor nanostructures with strong quantum confinement, the Auger effects are greatly enhanced by increased carrier−carrier interactions,[6] whereas thermal ionization is usually hindered by the increased spacing between successive energy states. The energy released from an Auger recombination process is given to another carrier in a single scattering event, usually with the participation of a phonon, whereas thermal ionization is a multiscattering process of a carrier with several phonons.[7] In the case of Auger autoionization or other ionization processes, the excess of a charge carrier in the NQD quenches the radiative recombination of the remaining electron−hole (e−h) pairs.[8] The general importance of Auger effects and ionization processes on the fluorescence and photoinduced absorption dynamics of NQDs has been discussed in several studies using different time-resolved techniques and rather different excitation densities.[9−16] Auger effects have been invoked to explain fluorescence and bleaching dynamics in ultrafast spectroscopy measurements.[17−20] Ionization processes are often referred to in the context of low densities and slow dynamics, such as the reversible PL quenching of single NQDs, manifested by "off" periods in the fluorescence under continuous-wave excitation.[8,21,22] However, the effect of the fast Auger recombination on the comparatively slow ionization processes and the implication on the PL dynamics of NQDs have not been treated so far, neither experimentally nor theoretically.

In this letter, we study the correlation between ionization processes and Auger recombination in NQDs and show that cooperative nonradiative effects dominate the fluorescence decay dynamics in the high-excitation-density regime. Spectrally resolved fluorescence decay measurements reveal a monotonic increase of the PL decay rate with excitation density. In the previously studied regime of low excitation densities, PL decay rates remain virtually unaffected, whereas under high-density excitation, in the multiple e−h pair regime, the PL decay rate rises. A kinematic analysis suggests that ionization processes are accelerated in the presence of Auger recombination (which occurs on much faster time scales), whereas previous rate equation models that do not consider the correlation between ionization and Auger recombination cannot reproduce our experimental observations.[6,8,17]

The proposed mechanism for a core/shell NQD is pictorially described in Figure 1. The most important ionization process is phonon-assisted tunneling to a trap state, whereas Auger autoionization is not energetically allowed for the lower energy carriers in the NQDs of this study, and thermal ionization is hindered by the high energy barrier (several eV) to the continuum. Phonon-assisted tunneling to a trap state becomes more probable for a carrier delocalized over the whole NQD (core and shell) than for a carrier delocalized only in the core because of the increased wave function overlap of carrier and trap states in the vicinity of the NQD's surface. Auger recombination results in a carrier occupying a higher energy level (Figure 1, middle sketch), which can either relax to a lower energy state or scatter to a trap state. These processes should not be treated as uncorrelated events because of the different ionization rates of carriers that undergo Auger recombination.

* Corresponding author: pavlos.lagoudakis@physik.uni-muenchen.de.

10.1021/jp053671y CCC: $30.25

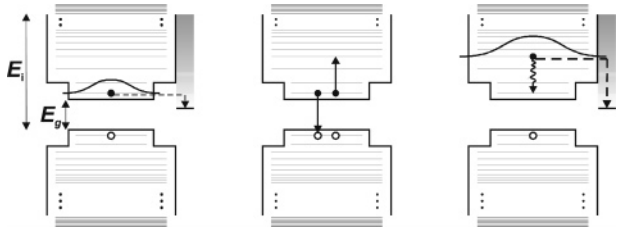

Figure 1. Elementary nonradiative effects in core/shell NQDs with band-gap energy E_g and carrier ionization energy E_i. A carrier from the ground state can be scattered to a trap by phonon-assisted tunneling (left sketch) or to a higher-energy state via an Auger recombination process (middle sketch). An excited carrier can relax energetically or alternatively can be more efficiently scattered to a trap via phonon-assisted tunneling due to increased carrier wave function overlap with the trap states in the vicinity of the NQD (right sketch).

In the right-hand sketch of Figure 1, the proposed Auger assisted ionization process is depicted, in which Auger recombination acts cooperatively with phonon-assisted tunneling to a trap state and results in a higher ionization rate. To experimentally observe this effect, we combine time-resolved PL, which has previously been described in the framework of Auger autoionization,[10,13] and high-density excitation above the one e−h population threshold, the effects of which have thus far only been considered on ultrafast time scales using PL upconversion and transient absorption.[17]

The quantum dots investigated in this study are CdSe/ZnS core/shell nanocrystals stabilized by hexadecylamine/trioctylphosphine/trioctylphosphine oxide ligands. The NQDs are of three different sizes, with mean core radii of 1.25, 1.55, and 2.45 nm. The nominal shell thickness is between 2 and 3 monolayers for all sizes, estimated from the added average mass of ZnS per particle and consistent with transmission electron microscopy measurements.[23] PL and absorption spectra from a solution of the biggest NQDs (core radius of 2.45 nm) in toluene are shown in the inset of Figure 2a. The standard deviation of the size distribution of these particles is 0.7 nm in radius as estimated from the inhomogeneous broadening of the emission spectra.[24] The PL quantum yield of these NQDs is ∼50% in solution. Time-resolved PL measurements were performed on 130-nm thick films of dispersed NQDs (average interparticle distance ∼30 nm) embedded in polystyrene using time-correlated single-photon counting of 1.2-ns resolution. The NQDs were excited nonresonantly with 130-fs pulses at 400 nm at room temperature under vacuum conditions. For the range of excitation densities used in this study (25−250 μJ/cm^2), the average number of e−h pairs per NQD $\langle N\rangle$ is calculated from $\langle N\rangle = J_p\sigma$, where J_p is the excitation photon flux and σ the NQD absorption cross-section.[25] Absorption from the shell has been neglected, since the excitation energy (3.1 eV) is much lower than the band gap of ZnS (3.6 eV).

Figure 2a shows two spectrally integrated PL decay curves obtained under different excitation densities (25 μJ/cm^2) and (250 μJ/cm^2). Apart from the nonexponential character of the decay dynamics of each curve, as expected from ensemble measurements due to the statistical distribution of decay lifetimes,[10] there is an apparent change of the PL decay rate for the different excitation densities. We ensured that no hysteresis occurred by measuring the excitation-density dependence for both increasing and decreasing densities. Decay rates are simply determined as the inverse of the 1/e decay time ($k_{1/e}$). No fitting curve is used throughout this study because of the manifold of distribution functions that affect the decay dynamics.

In semiconductor nanostructures, Auger effects strongly depend on the degree of spatial confinement.[6] Therefore, the

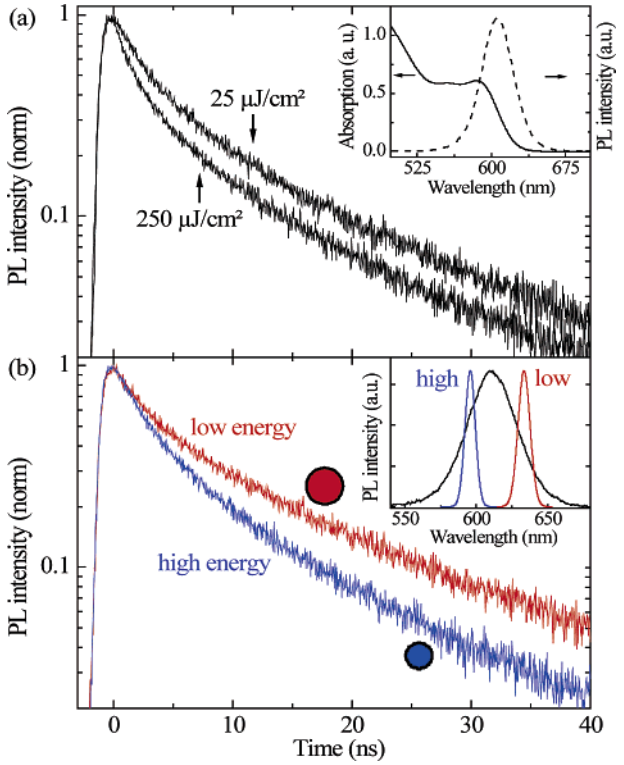

Figure 2. (a) Spectrally integrated PL decay curves of an ensemble of CdSe/ZnS core/shell NQDs at 25 μJ/cm^2 and 250 μJ/cm^2 excitation. Inset: Emission (dashed line) and absorption (solid line) spectra of CdSe/ZnS core/shell NQDs in solution. (b) Spectrally filtered PL decay curves measured under 25 μJ/cm^2 excitation at the high- and low-energy sides of the PL spectra. Inset: PL spectrum of a film of CdSe/ZnS NQDs (solid line). The colored lines show the transmission bandwidth of the filters employed.

distribution of NQD sizes in an ensemble impedes a quantitative interpretation of the recombination dynamics. Spectral filtering of the PL can substantially reduce the size distribution of NQDs involved in the dynamics. Interferometric filters are used to spectrally narrow the PL measured and consequently the distribution of NQD sizes. Spectrally filtered PL decay curves detected under the same excitation density (25 μJ/cm^2) are shown in Figure 2b. The PL signal is collected from the high- and low-energy sides of the emission maximum, which corresponds to NQDs of 2.35 and 3-nm core radius respectively, as indicated by the colored curves in the inset of Figure 2b.

In a qualitative picture, the dependence of PL decay on excitation density and NQD size can simply be attributed to Auger effects and ionization processes, following previous reports.[6,11,17] This view is further supported from the sublinear dependence of the integrated emission intensity with increasing excitation density shown in the inset of Figure 3. Hereafter, to gain quantitative insight into the different Auger processes or the possibility of other nonradiative decay channels that give rise to the observed PL dynamics, it is necessary to systematically measure the change of the PL decay rate over a wide range of excitation densities and thus e−h pair populations. Figure 3 shows the dependence of PL decay rate, $k_{1/e}$, on e−h pair population for both the high- and low-energy sides of the inhomogeneous size distribution. The decay rate increases monotonically with $\langle N\rangle$. Note that the absorption cross-section is larger for the large (i.e., lower-energy) NQDs, enabling greater $\langle N\rangle$ than for the smaller NQDs.

In NQDs, the most commonly investigated nonradiative processes are Auger recombination, Auger autoionization, thermal ionization, and phonon-assisted tunneling to a trap.[6−8]

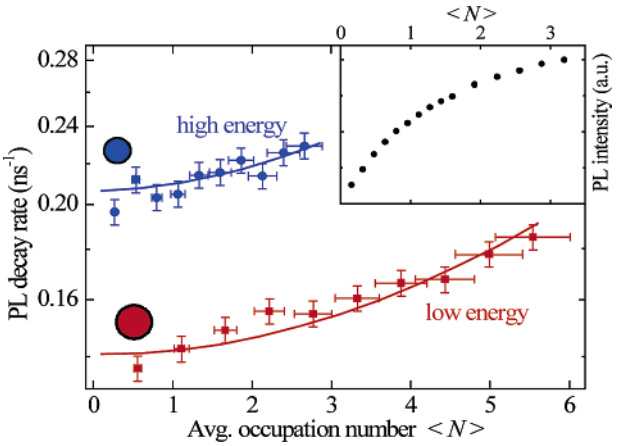

Figure 3. PL decay rate of the spectrally filtered emission vs average occupation number of e−h pairs per NQD. Squares (circles) correspond to the low (high)-energy side of the inhomogeneously broadened PL and thus to large (small) particles within the ensemble. Solid lines correspond to the theoretical results. Inset: Integrated PL intensity vs excitation density.

Whereas the Auger effects usually occur on the picosecond time scale, thermal ionization and phonon-assisted tunneling to a trap state are usually at least 1 order of magnitude slower and are thus generally neglected in the framework of ultrafast dynamics.[26,27] However, phonon-assisted tunneling to a trap state becomes more probable the higher the energy level is from which the carrier is ejected. Since Auger recombination excites a carrier to higher energy states, it increases the probability of carrier ionization, thus suggesting a correlation between the two effects.

Auger recombination becomes progressively faster as the number of e−h pairs N in the NQD increases ($k \propto N^2$). The discrete dependency of the Auger recombination rate k on N makes the representation of Auger recombination using number states most appropriate.[17] Under nonresonant excitation of an ensemble of NQDs with short pulses, number-state filling can be approximated by a Poissonian distribution, provided the average number $\langle N \rangle$ of e−h pairs per NQD is known. Note that $n_i\ (t = 0) \propto (\langle N \rangle^i/i!)e^{-\langle N \rangle}$, where n_i is the number of NQDs with i e−h pairs.

In the multiple e−h pair regime, radiative recombination can occur from any n_i state. However, because of the lower oscillator strength of the higher-energy states, the emission originates mostly from the lowest-energy e−h pair, independent of $\langle N \rangle$.[28] Auger electron cooling, an efficient thermalization process, thus renders occupation of the ground state most probable at all times in the multiple e−h pair regime,[7,18−20] whereas ionization processes quench the radiative recombination of the remaining e−h pairs because of the excess of a charge carrier in the NQD.[8] Considering these effects, the dynamics of nonresonantly excited NQDs can be approximated with the following set of number-state filling equations:

$$\frac{dn_i}{dt} = -(k_r + k_i)n_i + [(1 - P_a)k_{i+1} + k_r]n_{i+1}$$

where k_r is the effective radiative recombination rate, k_i (with $i \geq 2$) is the Auger recombination rate of the ith number state, and P_a is the probability of Auger assisted ionization. The schematic coupling between the number states and the different processes are depicted for the first three number states in Figure 4a. Here, we have assumed that one e−h and two e−h pair states have the same effective radiative recombination rate, k_r.[29] Each number state $i \geq 2$ can either recombine radiatively, in

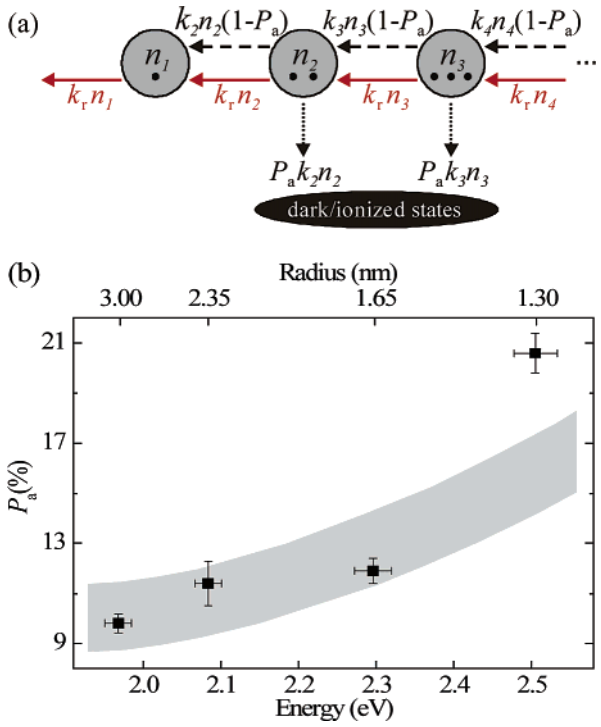

Figure 4. (a) Scheme of the different recombination pathways in the number-state picture for the first three number states (n_1, n_2, n_3). Each number state higher than 1 can either recombine radiatively, in which case it increases the immediate lower number state (k_rn_i, red arrows), or alternatively relax nonradiatively through Auger recombination. Some of the NQDs undergoing Auger recombination get ionized, which leads to the NQDs entering a dark state ($P_ak_in_i$, dotted arrows). The remaining NQDs increase the immediate lower number state following the rate $((1 - P_a)k_in_i$, dashed arrows). (b) The dependence of the Auger assisted ionization probability, P_a, on the emission energy of NQDs of different core radius. The horizontal error bars correspond to the full width at half-maximum of the detection bandwidth, the vertical error bars correspond to ±10% change of the rms value of the fit, and the gray area corresponds to the calculated tunneling probability (see text).

which case the subsequent lower number state is increased (k_rn_i, red arrows), or decay nonradiatively through Auger recombination (k_in_i). Of those e−h pairs that undergo Auger recombination, some lead to ionization and charging of the NQD ($P_ak_in_i$, dotted arrows), while the remainder increase the immediate lower number state ($(1 - P_a)k_in_i$, dashed arrows). The effective radiative rate k_r is extrapolated from Figure 3 for $\langle N \rangle \rightarrow 0$ and therefore includes all excitation-density-independent decay channels, while k_i is calculated from

$$k_i{:}k_2 = \left(\frac{i}{2}\right)^2, \quad \text{with } i > 2$$

where we have approximated $k_2 = 10 \cdot k_r$, and neglected the size dependence of this ratio.[17,30] The overall dynamics of the photon states dp/dt that accounts for the experimentally measured PL is given by

$$\frac{dp}{dt} = k_r \sum_{i=1}^{m} n_i$$

where m counts the participating number states. All number states with population ≥ 0.5% of the total number of e−h pairs are considered in the calculations. This set of number-state filling equations predicts the experimentally observed dependence of the PL decay rate on the excitation density for a probability of Auger assisted ionization, P_a, of 11.4% for the smaller and 9.8%

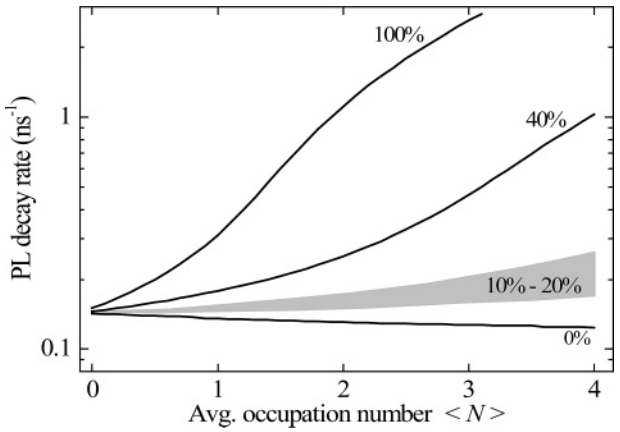

Figure 5. The calculated dependence of the PL decay rates on the average occupation number of e−h pairs per NQD for different probabilities of occurrence of Auger assisted ionization as tagged. The gray area corresponds to the experimentally identified region.

for the larger NQDs. The numerical results of the model are compared with the experimental data in Figure 3. Auger assisted ionization, P_a, is effectively the only fitting parameter in the introduced kinematic model that results in a good agreement with the experiment.

The next obvious step is to investigate the dependence of the Auger assisted ionization probability on the emission energy of NQDs of different core radius. The spectrally resolved PL decay of NQDs of core radii 1.3 and 1.65 nm (mean size selected by spectral filtering) was measured and characterized in the same way as with the larger NQDs presented above. An Auger assisted ionization probability is derived for each size. Figure 4b shows the dependence of the Auger assisted ionization probability P_a on the emission energy of the NQDs used in this study. Interestingly, the Auger assisted ionization probability increases with decreasing size of NQDs. This is expected qualitatively because of the increasing tunneling probability of a carrier to a trap state with decreasing size of the NQDs. The calculated tunneling probability of a carrier excited via Auger recombination to a trap state is superimposed as a gray stripe in Figure 4b with the Auger assisted ionization probability values derived from the experiment. For this calculation, a barrier thickness of 2.52 ± 0.1 Å is used. The effective mass of an electron in a CdSe/ZnS core/shell NQD is scaled for the different sizes of nanocrystals,[31] and the vacuum ionization energy is approximated to 6 eV,[32] both in agreement with the literature. It is reassuring for the validity of the straightforward theoretical model presented here that the Auger assisted ionization probability P_a, the only variable parameter of this model, follows the quantitatively expected dependency on NQD size and thus predicts correctly the experimental trends observed.

To underline the fundamental importance of Auger assisted ionization and Auger recombination, numerical simulations are performed for different probabilities P_a. The results for P_a varying from 0% to 100% are shown in Figure 5. Evidently, a simplified picture that does not account for Auger assisted ionization ($P_a = 0\%$) predicts a *decrease* in the PL decay rate with increasing excitation density. In contrast, a model that treats Auger assisted ionization as a certain consequence of Auger recombination results in a highly superlinear dependence. Apparently, the experimentally observed dependence of the PL decay rate on the average number of e−h pairs per NQD can be predicted when the occurrence of Auger assisted ionization is considered as a possible but not certain outcome of Auger recombination. This link demonstrates that Auger recombination and phonon-assisted tunneling cannot be thought of as uncorrelated events, congruently with previous reports.[33]

In conclusion, we have demonstrated that cooperative nonradiative effects, such as Auger recombination and phonon-assisted tunneling dominate the PL dynamics of NQDs and describe the intriguing increase in the PL decay rate above the average population of one e−h pair in the limit of strong electronic confinement.

Acknowledgment. We are indebted to W. Stadler and C. Holopirek for excellent technical assistance. Financial support of the EU HYTEC Network and the DFG through the SPP "Photonic Crystals", the SFB486 as well as a Gottfried Wilhelm Leibniz Preis is gratefully acknowledged.

References and Notes

(1) Yoffe, A. D. *Adv. Phys.* **2001**, *50*, 1.
(2) Woggon, U. *Optical Properties of Semiconductor Quantum Dots*; Springer: Berlin, 1997.
(3) Alivisatos, A. P. *Science* **1996**, *271*, 933.
(4) Klimov, V. I.; Mikhailovsky, A. A.; Su Xu; Malko, A.; Hollingsworth, J. A.; Leatherdale, C. A.; Eisler, H.-J.; Bawendi, M. G. *Science* **2000**, *290*, 314.
(5) Clapp, A. R.; Medintz, I. L.; Mauro, J. M.; Fisher, B. R.; Bawendi, M. G.; Mattoussi, H. *J. Am. Chem. Soc.* **2004**, *126*, 301.
(6) Chepic, D. I.; Efros, Al. L.; Ekimov, A. I.; Ivanov, M. G.; Kharchenko, V. A.; Kudriavtsev, I. A.; Yazeva, T. V. *J. Lumin.* **1990**, *47*, 113.
(7) Wang, L. W.; Califano, M.; Zunger, A.; Franceschetti, A. *Phys. Rev. Lett.* **2003**, *91*, 056404.
(8) Efros, Al. L.; Rosen, M. *Phys. Rev. Lett.* **1997**, *78*, 1110.
(9) Ghanassi, M.; Schanne-Klein, M. C.; Hache, F.; Ekimov, A. I.; Ricard, D.; Flytzanis, C. *Appl. Phys. Lett.* **1993**, *62*, 78.
(10) Schlegel, G.; Bohnenberger, J.; Potapova, I.; Mews, A. *Phys. Rev. Lett.* **2002**, *88*, 137401.
(11) Lomascolo, M.; Cretì, A.; Leo, G.; Vasanelli, L.; Manna, L. *Appl. Phys. Lett.* **2003**, *82*, 418.
(12) Neuhauser, R. G.; Shimizu, K. T.; Woo, W. K.; Empedocles, S. A.; Bawendi, M. G. *Phys. Rev. Lett.* **2000**, *85*, 3301.
(13) Fisher, B. R.; Eisler, H.-J.; Stott, N. E.; Bawendi, M. G. *J. Phys. Chem. B* **2004**, *108*, 143.
(14) Krauss, T. D.; O'Brien, S.; Brus, L. E. *J. Phys. Chem. B* **2001**, *105*, 1725.
(15) Roussignol, P.; Kull, M.; Ricard, D.; de Rougemont, F.; Frey, R.; Flytzanis, C. *Appl. Phys. Lett.* **1987**, *51*, 1882.
(16) Zheng, J. P.; Kwok, H. S. *Appl. Phys. Lett.* **1989**, *54*, 1.
(17) Klimov, V. I.; Mikhailovsky, A. A.; McBranch, D. W.; Leatherdale, C. A.; Bawendi, M. B. *Science* **2000**, *287*, 1011.
(18) Klimov, V. I.; McBranch, D. W.; Leatherdale, C. A.; Bawendi, M. B. *Phys. Rev. B* **1999**, *60*, 13740.
(19) Guyot-Sionnest, P.; Shim, M.; Matranga, C.; Hines, M. *Phys. Rev. B* **1999**, *60*, R2181.
(20) Klimov, V. I.; McBranch, D. W. *Phys. Rev. Lett.* **1998**, *80*, 4028.
(21) Verberk, R.; vanOijen, A. M.; Orrit, M. *Phys. Rev. B* **2002**, *66*, 233202.
(22) Müller, J.; Lupton, J. M.; Rogach, A. L.; Feldmann, J.; Talapin, D. V.; Weller, H. *Appl. Phys. Lett.* **2004**, *85*, 381.
(23) Talapin, D. V.; Rogach, A. L.; Kornowski, A.; Haase, M.; Weller, H. *Nano Lett.* **2001**, *1*, 207.
(24) Mikulec, F. V.; Kuno, M.; Bennati, M.; Hall, D. A.; Griffin, R. G.; Bawendi, M. G. *J. Am. Chem. Soc.* **2000**, *122*, 2532.
(25) Leatherdale, C. A.; Woo, W.-K.; Mikulec, F. V.; Bawendi, M. G. *J. Phys. Chem. B* **2002**, *106*, 7619.
(26) Labeau, O.; Tamarat, P.; Lounis, B. *Phys. Rev. Lett.* **2003**, *90*, 257404.
(27) Crooker, S. A.; Barrick, T.; Hollingsworth, J. A.; Klimov, V. I. *Appl. Phys. Lett.* **2003**, *82*, 2793.
(28) Efros, Al. L.; Rosen, M. *Annu. Rev. Mater. Sci.* **2000**, *30*, 475.
(29) Bacher, G.; Weigand, R.; Seufert, J.; Kulakovskii, V. D.; Gippius, N. A.; Forchel, A.; Leonardi, K.; Hommel, D. *Phys. Rev. Lett.* **1999**, *83*, 4417.
(30) Achermann, M.; Hollingsworth, J. A.; Klimov, V. I. *Phys. Rev. B* **2003**, *68*, 245302.
(31) Landolt-Börnstein *Numerical Data and Functional Relationship in Science and Technology, New Series, Group III*; Springer: Berlin, 1979; Vol. 17.
(32) Nethercot, A. H., Jr. *Phys. Rev. Lett.* **1974**, *33*, 1088.
(33) Kuno, M.; Fromm, D. P.; Johnson, S. T.; Gallagher, A.; Nesbitt, D. J. *Phys. Rev. B* **2003**, *67*, 125304.